Journal of Sound and Vibration 325 (2009) 583–596

Contents lists available at ScienceDirect

Journal of Sound and Vibration

journal homepage: www.elsevier.com/locate/jsvi

Aero-thermo-mechanical characteristics of imperfect shape memory alloy hybrid composite panels

Hesham Hamed Ibrahim [a,b,*], Hong Hee Yoo [a], Kwan-Soo Lee [a]

[a] Department of Mechanical Engineering, Hanyang University, Seoul 133-791, South Korea
[b] Space Division, National Authority for Remote Sensing and Space Sciences, Cairo 11769, Egypt

ARTICLE INFO

Article history:
Received 5 August 2008
Received in revised form
19 March 2009
Accepted 19 March 2009
Handling Editor: C.L. Morfey
Available online 22 April 2009

ABSTRACT

A nonlinear finite element model is provided to predict the static aero-thermal deflection and the vibration behavior of geometrically imperfect shape memory alloy hybrid composite panels under the combined effect of thermal and aerodynamic loads. The nonlinear governing equations are obtained using Marguerre curved plate theory and the principle of virtual work taking into account the temperature-dependence of material properties. The effect of large deflection is included in the formulation through the von Karman nonlinear strain–displacement relations. The thermal load is assumed to be a steady-state constant-temperature distribution, whereas the aerodynamic pressure is modeled using the quasi-steady first-order piston theory. The Newton–Raphson iteration method is employed to obtain the nonlinear aero-thermal deflections, while an eigenvalue problem is solved at each temperature step and static aerodynamic load to predict the free vibration frequencies about the deflected equilibrium position. Finally, the nonlinear deflection and free vibration characteristics of a composite panel are presented, illustrating the effects of geometric imperfection, temperature rise, aerodynamic pressure, boundary conditions and shape memory alloy fiber embeddings on the panel response.

1. Introduction

Composite plates are widely used in the external skin panels of high speed flight vehicles. The accurate prediction of the post-buckling response of these panels is of utmost importance, because these panels experience high temperatures due to aerodynamic heating, which can induce thermal buckling and may also results in a dynamic instability. In addition, the large thermal deflections of the skin panels can change its aerodynamic shape affecting reduction in the flight performance.

Many literature concerning thermal buckling and vibration of perfect plates have been reported. Among those, a comprehensive literature review on thermally induced flexure, buckling, and vibration of plates and shells was presented by Tauchart [1] and Thornton [2]. Gray and Mei [3] provided a finite element formulation for predicting thermal post-buckling behavior and free vibration of thermally buckled composite plates. An analytical solution for the thermal buckling and post-buckling behavior of a plate strip was presented by Jones and Mazumdar [4]. Shi et al. [5] adopted the finite element method to study the thermal buckling behavior of laminated composite plates under combined mechanical and thermal loads. Oh et al. [6] performed post-buckling and vibration analyses considering large thermo-piezo-elastic deflections for fully symmetric and partially eccentric piezo-laminated composite plates. Ibrahim et al. [7] investigated the

* Corresponding author at: Space Division, National Authority for Remote Sensing and Space Sciences, Cairo 11769, Egypt. Tel.: +20 100 923 079.
E-mail addresses: hhibrahim76@hotmail.com (H.H. Ibrahim), hhyoo@hanyang.ac.kr (H.H. Yoo), ksleehy@hanyang.ac.kr (K.-S. Lee).

0022-460X/$ - see front matter © 2009 Elsevier Ltd. All rights reserved.
doi:10.1016/j.jsv.2009.03.027

thermal buckling and flutter boundaries of functionally graded material plates at elevated temperature. They adopted an incremental finite element technique to capture the effect of the temperature-dependence of material properties on the panel response. Ibrahim et al. [8] presented a finite element solution for the thermal buckling and nonlinear flutter performance of thin functionally graded material panels under combined aerodynamic and thermal loads. To account for the temperature-dependence of material properties, the thermal strain was modeled as an integral quantity of thermal expansion coefficient with respect to temperature. Ibrahim et al. [9] provided a finite element formulation to study the vibration behavior of functionally graded panels at elevated temperatures.

Shape memory alloys (SMA) have a unique ability to completely recover large pre-strains (up to 10 percent elongation) when heated above certain characteristic temperature. During the shape recovery process, a large tensile recovery stress occurs if the SMA is restrained. Both the recovery stresses and Young's modules of SMA exhibit nonlinear temperature-dependent properties. Birman [10] presented a comprehensive review on the literature concerning SMA up to 1997. Lee and Lee [11] utilized ABAQUS code to perform a numerical simulation for the buckling and postbuckling behavior of laminated composite shells with embedded shape memory alloy (SMA) wires. Tawfik et al. [12] proposed a novel concept in enhancing the thermal buckling and aeroelastic behavior of plates through embedding SMA fibers in it. Roh et al. [13] investigated the thermal post-buckling responses of shape memory alloy hybrid composite shell panels using a finite element method formulated on the basis of the layerwise theory. They utilized the cylindrical arc-length method to take account of the snapping phenomenon which is an unstable behavior observed in the shell panels. Park et al. [14] investigated the nonlinear vibration behavior of thermally buckled composite plates embedded with shape memory alloy fibers. An incremental method was adopted to account for the temperature dependent material properties. Ibrahim et al. [15] studied the thermal buckling and free vibration behavior of shape memory alloy hybrid composite (SMAHC) panels. Ibrahim et al. [16] investigated the thermal buckling and the acoustic response of shape memory alloy hybrid composite panels under combined thermal and random acoustic loads.

Since composite structures are usually fabricated at high temperatures, residual stresses and geometric imperfection are usually produced after the material is cooled to room temperature. A small initial geometric imperfection are widely known to have a detrimental effect on the buckling strength of plates, and to be the reason for the discrepancy between experimental buckling loads and theoretical predictions based on the perfect geometry. Therefore, many investigations are conducted on the stability analysis and free vibration of imperfect structures. Shi et al. [17] adopted a finite element modal method to solve the problem of thermal post-buckling of composite plates with initial imperfections. Shen [18] employed a perturbation technique and an iterative numerical procedure to study the thermal post-buckling imperfect laminated plates resting on an elastic foundation subjected to a uniform temperature rise. Girish and Ramachandra [19] investigated the free vibration behavior of thermally buckled laminated composite plates with geometric imperfections. Shariat and Eslami [20] provided a closed form solution for the critical buckling temperature change of an imperfect functionally graded plate using classical plate theory. Mirzavand and Eslami [21] presented a closed form solution for the critical buckling temperature change of functionally graded cylindrical shells using the Wan-Donnell model for initial imperfections. They utilized the first-order classical shell theory along with the Sanders nonlinear kinematic relations. Chen and Hsu [22] employed a perturbation technique to study the nonlinear vibration of initially stressed imperfect isotropic plates. Shen [23] employed a two-step perturbation technique to determine the buckling temperature and post-buckling equilibrium paths for an imperfect shear deformable FGM plate with temperature-dependent properties. However, to the best of authors' knowledge, the buckling and free vibration behaviors of imperfect composite panels under combined aerodynamic and thermal loads have not been accomplished in the literature. As the use of SMAHC panels is expected to increase, it is worth investigating the effect of SMA fiber embeddings on the behavior of an imperfect composite panel.

In this work, a nonlinear finite element model is presented for the aero-thermal buckling and free vibration behavior of an imperfect SMAHC panels under combined thermal and aerodynamic loads. The nonlinear governing equations for a thin, imperfect rectangular panel are obtained using Marguerre curved plate theory, von Karman strain–displacement relations, and the principle of virtual work. To account for the temperature-dependence of material properties, the thermal strain is modeled as an integral quantity of the thermal expansion coefficient with respect to temperature [8]. The thermal load is assumed to be a steady-state constant-temperature distribution, whereas the aerodynamic pressure is modeled using the quasi-steady first-order piston theory. Noting that, to the best of authors' knowledge, the theoretical development of the Marguerre curved plate theory along with the finite element solution for the analysis of imperfect laminates and its application, in the manner described in the current work, have not been attempted so far elsewhere. Finally, numerical results are provided to show the effects of the geometric imperfection, temperature rise, aerodynamic pressure, boundary conditions and shape memory alloy fiber embeddings on the panel response.

2. Finite element formulation

2.1. Nonlinear strain–displacement relations

The nodal degrees of freedom vector $\{\theta\}$ of a rectangular four-nodded Bogner–Fox–Schmidt (BFS) C^1 conforming plate element having 6 degrees of freedom at each node can be written as [24]

$$\boldsymbol{\theta} = \left\{ \left\{ w, \frac{\partial w}{\partial x}, \frac{\partial w}{\partial y}, \frac{\partial^2 w}{\partial x \partial y} \right\}, \{u, v\} \right\}^{\mathrm{T}} = \left\{ \begin{array}{c} \mathbf{w}_b \\ \mathbf{w}_m \end{array} \right\} \tag{1}$$

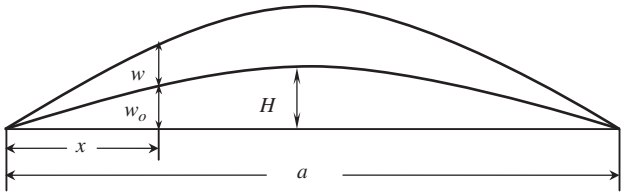

Fig. 1. Schematic for the geometric imperfection w_0 and the transverse deflection w.

where $\mathbf{w}_b$ is the nodal transverse displacement and rotations vector and $\mathbf{w}_m$ is the nodal membrane displacements vector. Consider the initial geometric imperfection w_0 and the transverse deflection w shown in Fig. 1, the Marguerre curved plate strain–displacement relation along with von Karman large deflection can be written as [25]

$$\begin{Bmatrix} \varepsilon_x \\ \varepsilon_y \\ \gamma_{xy} \end{Bmatrix} = \begin{Bmatrix} \dfrac{\partial u}{\partial x} \\ \dfrac{\partial v}{\partial y} \\ \dfrac{\partial u}{\partial y} + \dfrac{\partial v}{\partial x} \end{Bmatrix} + \begin{Bmatrix} \dfrac{1}{2}\left(\dfrac{\partial w}{\partial x}\right)^2 \\ \dfrac{1}{2}\left(\dfrac{\partial w}{\partial y}\right)^2 \\ \dfrac{\partial w}{\partial x}\dfrac{\partial w}{\partial y} \end{Bmatrix} + \begin{Bmatrix} \dfrac{\partial w}{\partial x}\dfrac{\partial w_0}{\partial x} \\ \dfrac{\partial w}{\partial y}\dfrac{\partial w_0}{\partial y} \\ \dfrac{\partial w}{\partial x}\dfrac{\partial w_0}{\partial y} + \dfrac{\partial w_0}{\partial x}\dfrac{\partial w}{\partial y} \end{Bmatrix} + z \begin{Bmatrix} -\dfrac{\partial^2 w}{\partial x^2} \\ -\dfrac{\partial^2 w}{\partial y^2} \\ -2\dfrac{\partial^2 w}{\partial x \partial y} \end{Bmatrix} \tag{2}$$

Or in a compact form as

$$\boldsymbol{\varepsilon} = \boldsymbol{\varepsilon}_m + \boldsymbol{\varepsilon}_b + \boldsymbol{\varepsilon}_{w_0} + z\boldsymbol{\kappa} \tag{3}$$

$\boldsymbol{\varepsilon}_m, \boldsymbol{\varepsilon}_b, \boldsymbol{\varepsilon}_{w_0}$, and $\boldsymbol{\kappa}$ are the membrane linear strain vector, the membrane nonlinear strain vector, inplane strain vector due to geometric imperfection and the bending strain vector, respectively.

The European standard for steel structures requires that when a geometrically nonlinear elastic or elastic-plastic analysis with explicit representation of imperfections is used in design, a range of potentially damaging imperfection forms should be explored if the most unfavorable imperfection form cannot be readily identified. This code also recommends that the imperfection should be specified in the form of the critical buckling mode from a linear buckling analysis, with the amplitude linked to the fabrication quality, unless a different unfavorable pattern is justified [26]. Accordingly, the initial geometric imperfection is assumed to have the form:

$$w_0 = H \sin\frac{n\pi x}{a} \sin\frac{m\pi y}{b} \tag{4}$$

where n, m are the number of half waves, while a, b are the panel dimensions along x- and y-directions, respectively.

2.2. Constitutive equations

For the kth composite lamina impregnated with SMA fibers, the stress–strain relations can be expressed as [16]

$$\boldsymbol{\sigma}^k = \begin{Bmatrix} \sigma_x^k \\ \sigma_y^k \\ \tau_{xy}^k \end{Bmatrix} = \overline{\mathbf{Q}}^k(T)\boldsymbol{\varepsilon} + V_s^k \boldsymbol{\sigma}_r^k(T) - V_m^k \int_{T_{\text{ref}}}^{T} \overline{\mathbf{Q}}_m^k(\tau)\boldsymbol{\alpha}_m^k(\tau)\,\mathrm{d}\tau \tag{5}$$

where $\boldsymbol{\sigma}$ and $\boldsymbol{\sigma}_r$ are the inplane and the SMA constrained shape recovery stress vectors at a given temperature T. V_m and V_s are the volume fractions of the composite matrix and SMA fibers, respectively. In addition, $\boldsymbol{\alpha}_m$, $\overline{\mathbf{Q}}$ and $\overline{\mathbf{Q}}_m$ are the thermal expansion coefficient vector of the composite matrix, the transformed reduced stiffness matrix of the SMA embedded lamina, and the transformed reduced stiffness matrix of the composite matrix, respectively. Note that the SMA fibers are embedded in same direction of the composite matrix fibers, and assumed uniformly distributed within each layer. Integrating Eq. (5) over the plate thickness h, the constitutive equation is obtained as

$$\begin{Bmatrix} \mathbf{N} \\ \mathbf{M} \end{Bmatrix} = \begin{bmatrix} \mathbf{A} & \mathbf{B} \\ \mathbf{B} & \mathbf{D} \end{bmatrix} \begin{Bmatrix} \boldsymbol{\varepsilon}_m^o + \boldsymbol{\varepsilon}_b^o + \boldsymbol{\varepsilon}_{w_0}^o \\ \boldsymbol{\kappa} \end{Bmatrix} - \begin{Bmatrix} \mathbf{N}_T \\ \mathbf{M}_T \end{Bmatrix} + \begin{Bmatrix} \mathbf{N}_r \\ \mathbf{M}_r \end{Bmatrix} \tag{6}$$

where

$$\begin{Bmatrix} \mathbf{N}_T \\ \mathbf{M}_T \end{Bmatrix} = V_m \int_{-h/2}^{h/2} \left(\int_{T_{\text{ref}}}^{T} \mathbf{Q}_m^k(\tau)\boldsymbol{\alpha}_m^k(\tau)\,\mathrm{d}\tau \right) \begin{Bmatrix} 1 \\ z \end{Bmatrix} \mathrm{d}z, \quad \begin{Bmatrix} \mathbf{N}_r \\ \mathbf{M}_r \end{Bmatrix} = V_s \int_{-h/2}^{h/2} \boldsymbol{\sigma}_r \begin{Bmatrix} 1 \\ z \end{Bmatrix} \mathrm{d}z$$

2.3. Aerodynamic pressure loading

The aerodynamic pressure caused by a supersonic airflow will be approximated by the first-order quasi-steady piston theory [12], which is valid for $\sqrt{2}<M_\infty$ and shows good accuracy in the range of $\sqrt{2}<M_\infty<5$, where M_∞ is the Mach number. The aerodynamic pressure using the first-order piston theory is expressed as

$$P_a = -\left(\frac{g_a}{\omega_0}\frac{D_{110}}{a^4}\frac{\partial w}{\partial t} + \lambda\frac{D_{110}}{a^3}\frac{\partial(w+w_0)}{\partial x}\right) \tag{7}$$

where

$$g_a = \sqrt{\lambda \mathbf{C_a}}, \quad \mathbf{C_a} = \frac{(M_\infty^2-2)^2}{(M_\infty^2-1)^2}\frac{\rho_a a}{\rho h \beta}, \quad \lambda = \frac{2qa^3}{\beta D_{110}},$$
$$q = \frac{\rho_a v^2}{2}, \quad \beta = \sqrt{M_\infty^2-1} \quad \text{and} \quad \omega_0 = \left(\frac{D_{110}}{\rho h a^4}\right)^{1/2}$$

where P_a is the aerodynamic pressure loading, v is the airflow velocity on one side of the panel, q is the dynamic pressure, ρ and ρ_a is the panel and air mass densities, g_a is the non-dimensional aerodynamic damping, C_a is the aerodynamic damping coefficient, λ is the non-dimensional dynamic pressure, D_{110} is the first entry in the flexural stiffness matrix $\mathbf{D}(1,1)$ when all the fibers of the composite layers are aligned in the airflow x-direction, and a is the stream wise panel length.

2.4. Governing equations

By using the principle of virtual work and Eqs. (2) and (6), the nonlinear governing equations can be derived as follows:

$$\delta\text{Work} = \delta\text{Work}_{\text{int}} - \delta\text{Work}_{\text{ext}} = 0 \tag{8}$$

where the virtual work done by internal stresses can be written as

$$\begin{aligned}\delta\text{Work}_{\text{int}} &= \int_A (\delta(\boldsymbol{\varepsilon}_m + \boldsymbol{\varepsilon}_b + \boldsymbol{\varepsilon}_{w_0})^{\mathrm{T}} N + \delta\boldsymbol{\kappa}^{\mathrm{T}}\mathbf{M})\,\mathrm{d}A \\ &= \delta\boldsymbol{\theta}^{\mathrm{T}}\left(\mathbf{k} + \mathbf{k}_{w_0} - \mathbf{k}_T + \mathbf{k}_r + \frac{1}{2}(\mathbf{n}1 + \mathbf{n}_{w_0}) + \frac{1}{3}\mathbf{n}2\right)\boldsymbol{\theta} - \delta\boldsymbol{\theta}^{\mathrm{T}}(\mathbf{p}_T + \mathbf{p}_{Tw_0} - \mathbf{p}_r - \mathbf{p}_{rw_0})\end{aligned} \tag{9}$$

where $\mathbf{k}$, $\mathbf{k}_T$ and $\mathbf{k}_r$ are the linear, thermal and recovery stress stiffness matrices; $\mathbf{k}_{w_0}$ is a linear stiffness matrix due to geometric imperfection; $\mathbf{n}1$ and $\mathbf{n}2$ are the first- and second-order nonlinear stiffness matrices, respectively; $\mathbf{n}1_{w_0}$ is a first-order stiffness matrix due to geometric imperfection. In addition, $\mathbf{p}_T$ and $\mathbf{p}_r$ are thermal and recovery stress load vectors, and $\mathbf{p}_{tw_0}$ and $\mathbf{p}_{rw_0}$ are thermal and recovery load vectors due to initial geometric imperfection. On the other hand, the external virtual work $\delta\text{Work}_{\text{ext}}$ is given as [12]

$$\begin{aligned}\delta\text{Work}_{\text{ext}} &= \int_A\left(\delta w\left(-\rho h\frac{\partial^2 w}{\partial t^2} + P_a\right) + \delta u\left(-\rho h\frac{\partial^2 u}{\partial t^2}\right) + \delta v\left(-\rho h\frac{\partial^2 v}{\partial t^2}\right)\right)\mathrm{d}A \\ &= -\delta\boldsymbol{\theta}^{\mathrm{T}}\begin{bmatrix}\mathbf{m}_b & \mathbf{0}\\ \mathbf{0} & \mathbf{m}_m\end{bmatrix}\ddot{\boldsymbol{\theta}} - \delta\boldsymbol{\theta}^{\mathrm{T}}\begin{bmatrix}\mathbf{g}_b & \mathbf{0}\\ \mathbf{0} & \mathbf{0}\end{bmatrix}\dot{\boldsymbol{\theta}} - \delta\boldsymbol{\theta}^{\mathrm{T}}\lambda\begin{bmatrix}\mathbf{a}_{ab} & 0\\ 0 & 0\end{bmatrix}\boldsymbol{\theta} - \boldsymbol{\delta\theta}^{\mathrm{T}}\lambda\begin{Bmatrix}\mathbf{p}^{\text{sal}}\\ 0\end{Bmatrix} \\ &= -\delta\boldsymbol{\theta}^{\mathrm{T}}\mathbf{m}\ddot{\boldsymbol{\theta}} - \delta\boldsymbol{\theta}^{\mathrm{T}}\mathbf{g}\dot{\boldsymbol{\theta}} - \delta\boldsymbol{\theta}^{\mathrm{T}}\lambda\mathbf{a}_a\boldsymbol{\theta} - \delta\boldsymbol{\theta}^{\mathrm{T}}\lambda\mathbf{p}^{\text{sal}}\end{aligned} \tag{10}$$

where

$$\lambda\mathbf{a}_{ab} = \lambda\frac{D_{110}}{a^3}\int_A\left(\delta w\left(\frac{\partial w}{\partial x}\right)\right)\mathrm{d}A$$

$$\mathbf{g}_b = \frac{g_a}{\omega_0}\frac{D_{110}}{a^4}\int_A\left(\delta w\left(\frac{\partial w}{\partial t}\right)\right)\mathrm{d}A$$

$$\lambda\mathbf{p}_b^{\text{sal}} = \lambda\frac{D_{110}}{a^3}\int_A\left(\delta w\left(\frac{\partial w_0}{\partial x}\right)\right)\mathrm{d}A$$

$\mathbf{m}$, $\mathbf{g}$ and $\mathbf{a}_a$ are mass, aerodynamic damping, and aerodynamic stiffness matrices, respectively. $\mathbf{p}^{\text{sal}}$ is a static aerodynamic load vector which is function of the initial geometric imperfection w_0. By substituting Eqs. (9) and (10) into Eq. (8), the governing equations for an imperfect shape memory alloy hybrid composite plate under the combined action of thermal

and aerodynamic loads, can be written as

$$\mathbf{M}\ddot{\mathbf{W}} + \mathbf{G}\dot{\mathbf{W}} + \left(\lambda\mathbf{A}_a + \mathbf{K} + \mathbf{K}_{w_0} - \mathbf{K}_T + \mathbf{K}_r + \frac{1}{2}(\mathbf{N1} + \mathbf{N1}_{w_0}) + \frac{1}{3}\mathbf{N2}\right)\mathbf{W} = \mathbf{P}_T + \mathbf{P}_{Tw_0} - \mathbf{P}_r - \mathbf{P}_{rw_0} - \lambda\mathbf{P}^{\mathrm{sal}} \tag{11}$$

3. Solution procedures

3.1. Static aero-thermal deflection

For the static aero-thermal buckling problem, Eq. (11) reduces to

$$\left(\lambda\mathbf{A}_a + \mathbf{K} + \mathbf{K}_{w_0} - \mathbf{K}_T + \mathbf{K}_r + \frac{1}{2}(\mathbf{N1} + \mathbf{N1}_{w_0}) + \frac{1}{3}\mathbf{N2}\right)\mathbf{W}_s = \mathbf{P}_T + \mathbf{P}_{Tw_0} - \mathbf{P}_r - \mathbf{P}_{rw_0} - \lambda\mathbf{P}^{\mathrm{sal}} \tag{12}$$

where the subscripts a, T, r, and s stand for aerodynamic, thermal, recovery stress, and static, respectively. The solution procedure using Newton–Raphson method is presented in the following. Introducing the function $\Psi(\mathbf{W}_s)$ to Eq. (12) to be [27]

$$\Psi(\mathbf{W}_s) = \left(\lambda\mathbf{A}_a + \mathbf{K} + \mathbf{K}_{w_0} - \mathbf{K}_T + \mathbf{K}_r + \frac{1}{2}(\mathbf{N1} + \mathbf{N1}_{w_0}) + \frac{1}{3}\mathbf{N2}\right)\mathbf{W}_s - \mathbf{P}_T - \mathbf{P}_{Tw_0} + \mathbf{P}_r + \mathbf{P}_{rw_0} + \lambda\mathbf{P}^{\mathrm{sal}} = 0 \tag{13}$$

Eq. (13) can be written in the form of a truncated Taylor series expansion as

$$\Psi(\mathbf{W}_s + \delta\mathbf{W}) = \Psi(\mathbf{W}_s) + \frac{\mathrm{d}\Psi(\mathbf{W}_s)}{\mathrm{d}\mathbf{W}_s}\delta\mathbf{W} \cong 0 \tag{14}$$

where

$$\frac{\mathrm{d}\Psi(\mathbf{W}_s)}{\mathrm{d}\mathbf{W}_s} = (\lambda\mathbf{A}_a + \mathbf{K} + \mathbf{K}_{w_0} - \mathbf{K}_T + \mathbf{K}_r + \mathbf{N1} + \mathbf{N1}_{w_0} + \mathbf{N2}) = \mathbf{K}_{\tan} \tag{15}$$

Thus, the Newton–Raphson iteration procedure for the determination of the post-buckling deflection can be expressed as follows:

$$\Psi(\mathbf{W}_s)_i = \left(\lambda\mathbf{A}_a + \mathbf{K} + \mathbf{K}_{w_0} - \mathbf{K}_T + \mathbf{K}_r + \frac{1}{2}(\mathbf{N1} + \mathbf{N1}_{w_0})_i + \frac{1}{3}(\mathbf{N2})_i\right)(\mathbf{W}_s)_i - \mathbf{P}_T - \mathbf{P}_{Tw_0} + \mathbf{P}_r + \mathbf{P}_{rw_0} + \lambda\mathbf{P}^{\mathrm{sal}}$$

$$(\mathbf{K}_{\tan})_i(\delta\mathbf{W})_{i+1} = -\Psi(\mathbf{W}_s)_i$$

$$\delta\mathbf{W}_{i+1} = -\mathbf{K}_{\tan}^{-1}\Psi(\mathbf{W}_s)_i$$

$$(\mathbf{W}_s)_{i+1} = (\mathbf{W}_s)_i + (\delta\mathbf{W})_{i+1}$$

Convergence occurs in the above procedure when the maximum value of $\delta\mathbf{W}_{i+1}$ becomes less than a given tolerance $\varepsilon_{\mathrm{tol}}$, i.e. $\max|\delta\mathbf{W}_{i+1}| \leqslant \varepsilon_{\mathrm{tol}}$.

3.2. Free vibration

Once the panel buckling equilibrium position $\mathbf{W}_s$ is obtained for a certain temperature rise ΔT, the linear vibration frequency of the SMAHC panel about this equilibrium position can be determined. The solution of the differential Eq. (11) is the sum of a time-dependent homogeneous solution $\mathbf{W}_t$ and a time-independent particular solution $\mathbf{W}_s$ as follows [27]:

$$\mathbf{W} = \mathbf{W}_s + \mathbf{W}_t \tag{16}$$

Substituting Eq. (16) into Eq. (11) results in the following equation:

$$\mathbf{M}\ddot{\mathbf{W}}_t + \mathbf{G}\dot{\mathbf{W}}_t + \left(\lambda\mathbf{A}_a + \mathbf{K} + \mathbf{K}_{w_0} - \mathbf{K}_T + \mathbf{K}_r + \frac{1}{2}((\mathbf{N1})_{s+t} + (\mathbf{N1}_{w_0})_{s+t}) + \frac{1}{3}(\mathbf{N2})_{s+t}\right)(\mathbf{W}_s + \mathbf{W}_t) = \mathbf{P}_T + \mathbf{P}_{Tw_0} - \mathbf{P}_r - \mathbf{P}_{rw_0} - \lambda\mathbf{P}^{\mathrm{sal}} \tag{17}$$

where subscripts s and t, denote that the corresponding nonlinear stiffness matrix is evaluated by using $\mathbf{W}_s$ or $\mathbf{W}_t$. From Eq. (17), the equation of free vibration of a thermally buckled SMAHC panel can be stated as follows [27]:

$$\mathbf{M}\ddot{\mathbf{W}}_t + (\lambda\mathbf{A}_a + \mathbf{K} + \mathbf{K}_{w_0} - \mathbf{K}_T + \mathbf{K}_r + (\mathbf{N1})_s + (\mathbf{N1}_{w_0})_s + (\mathbf{N2})_s)\mathbf{W}_t = 0 \tag{18}$$

Table 1
Material properties of composite matrix and SMA fiber.

Nitinol	Graphite-epoxy	
See Figs. 2 and 3 for Young's modulus and recovery stresses	$\mathbf{E}1$	$155(1-6.35\times10^{-4}\,\Delta T)$ GPa
	$\mathbf{E}2$	$8.07(1-7.69\times10^{-4}\,\Delta T)$ GPa
$\mathbf{G}$ 25.6 GPa	$\mathbf{G}12$	$4.55(1-1.09\times10^{-3}\,\Delta T)$ GPa
$\boldsymbol{\rho}$ 6450 kg/m^3	$\boldsymbol{\rho}$	1550 kg/m^3
$\boldsymbol{\nu}$ 0.3	$\boldsymbol{\nu}$	0.22
$\boldsymbol{\alpha}$ 10.26×10^{-6}/°C	$\boldsymbol{\alpha}1$	$-0.07\times10^{-6}(1-0.69\times10^{-3}\,\Delta T)$/°C
	$\boldsymbol{\alpha}2$	$30.6\times10^{-6}(1+0.28\times10^{-4}\,\Delta T)$/°C

This can be written as

$$\mathbf{M}\ddot{\mathbf{W}}_t + \mathbf{K}_{\tan}\mathbf{W}_t = 0 \tag{19}$$

Assuming the solution of the above differential equation to take the following form:

$$\mathbf{W}_t = \bar{c}\boldsymbol{\Phi}e^{\Omega t} \tag{20}$$

By substituting this harmonic form into Eq. (19), a generalized eigenvalue problem can be stated as

$$(\Omega^2\mathbf{M} + \mathbf{K}_{\tan})\boldsymbol{\Phi} = 0 \tag{21}$$

Thus, the solution procedure comprises the evaluation of the static aero-thermal deflection and the associated stiffness matrices by following the Newton–Raphson iteration procedure outlined in the preceding section, and then, solving the eigenvalue problem of Eq. (21) for the natural frequencies Ω of a thermally buckled SMAHC panel with initial geometric imperfection.

4. Numerical results and discussions

Aero-thermal post-buckling and natural vibration behavior of an imperfect laminated composite panel with and without SMA fibers is presented. The panel is modeled using a 10×10 mesh. A traditional clamped composite panel and a SMAHC panel with 10 percent volume fraction and 3 percent pre-strain are studied and compared. Panel edges are assumed all simply supported or all clamped. The panel dimensions and stacking sequence adopted in this study are $0.3\times0.3\times0.0012$ (m) and $[0/-45/45/90]_s$ The amplitude H of the initial sinusoidal geometric imperfection was chosen to be 0.1 times the plate thickness h. Uniform temperature change was applied to the plate, and the reference temperature is assumed to be 21 °C in this study. Table 1 presents the material properties of the composite matrix and SMA fiber [16], while the variation of the modulus of elasticity and recovery stress of a trained Nitinol are presented in Figs. 2 and 3 [28].

4.1. Validation of the formulation

Fig. 4 shows the thermal post-buckling equilibrium paths for simply supported, eight-layered symmetric cross ply $[0/90/90/0]_s$ graphite-epoxy laminate with three different aspect ratios and subjected to a uniform temperature distribution. The curves are shown for perfect plate ($w_0 = 0$) and also for a plate with an initial sinusoidal geometric imperfection with the value of H equals 0.1 times the plate thickness h. The length of the plate, a, is kept constant and $a/h = 250$. The temperatures have been normalized by T_{cr}, the buckling temperature of a square laminate. It is seen that increasing the plate aspect ratio, results in increasing the critical buckling temperatures, and also results in a more pronounced difference between the perfect plate response and the imperfect one. Moreover, due to the presence of the initial imperfection, bifurcation buckling does not take place, because any small temperature rise results in a prompt transverse deflection of the imperfect panel. To validate the present formulation, the results presented in Fig. 4 were compared to those of Fig. 6 in Ref. [19] and were found to be in a good agreement.

4.2. Aero-thermal deflection

The panel static response under combined thermal and aerodynamic loads is investigated hereinafter, illustrating the effect of an initial sinusoidal geometric imperfection with different half wave numbers. First, the thermal buckling sensitivity to geometric imperfection will be studied for both simply supported and clamped composite panels. Then, the composite panel will be impregnated with pre-strained SMA fibers to show the impact of constrained shape recovery process on the panel thermal stability. Finally, an airflow of $\lambda = 50$ will be imposed to the composite panel to illustrate the effect of geometric imperfection on the aero-thermal behavior of such panels. Fig. 5 presents the thermal post-buckling deflection of a composite panel with all edges clamped illustrating the effect of having a sinusoidal imperfection with multiple half wave numbers in both x- and y-directions. It is seen in the figure that, for symmetric and anti-symmetric

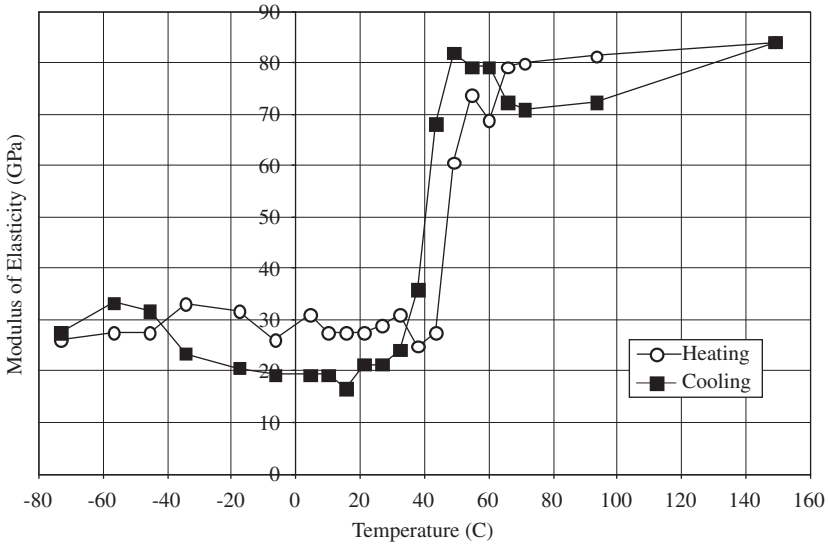

Fig. 2. Modulus of elasticity variation with temperature for a trained Nitinol fiber.

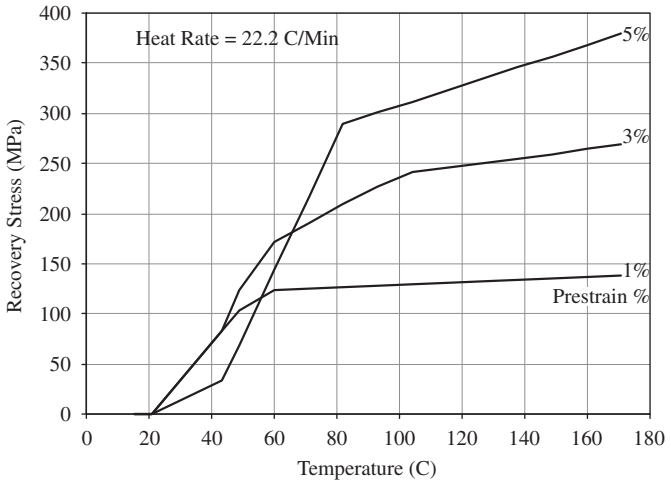

Fig. 3. Nitinol recovery stress as a function of both temperature and pre-strain percentage.

imperfections, there is no sudden out-of-plane deflection, i.e. buckling phenomenon, because any small temperature rise results in a prompt transverse deflection which is not favorable regarding aerodynamic performance. For symmetric imperfection shapes with half wave numbers higher than unity, the panel is seen to have a pseudo-buckling behavior with different thermal post-buckling deflections compared to the perfect panel. Moreover, by increasing the number of half waves up to 5, the post-buckling deflections turn to be lower than that of the perfect panel. For anti-symmetric imperfection shapes, the imperfect panel response is seen approaching the perfect one, and turns to be almost identical by increasing the number of half waves up 4. In the nonlinear region, it was found that increasing the temperature rise value results in a nonlinear increase in the post-buckling deflection **W**. Accordingly, the effect of the initial imperfection through the nonlinear stiffness matrix $\mathbf{N1}_{w_0}$ is expected to be more pronounced in the high temperature region. Moreover, since the $\mathbf{P}_{Tw_0}$ and $\mathbf{P}_{rw_0}$ load vectors are nonlinearly dependent on the temperature, their effect on the system will be more pronounced in the high temperature region too. Fig. 6 shows the effect of having multiple half waves in the *x*-direction only while having single half wave in the *y*-direction. It is found that no change in the behavior of anti-symmetric imperfection shapes is noticed compared to Fig. 5. While, all symmetric shapes show a prompt transverse deflection at the very beginning of the temperature rise.

Fig. 7 presents the thermal post-buckling deflection of a composite panel with all edges simply supported, while having a sinusoidal imperfection with multiple half wave numbers in both *x*- and *y*-directions. Panels with anti-symmetric imperfection shapes continue to show almost the same response as that of the perfect one. It is also found that the

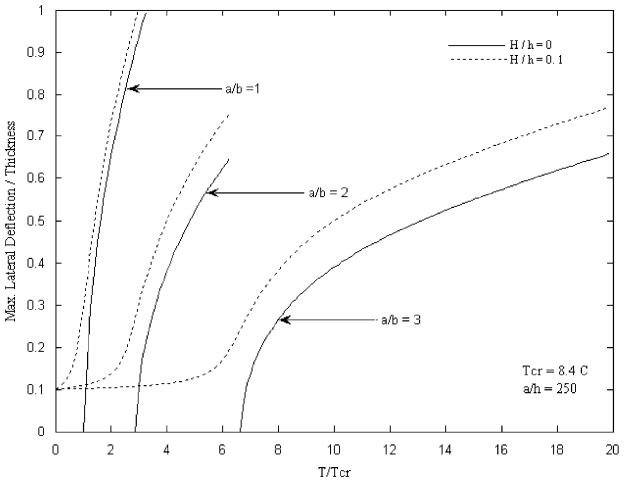

Fig. 4. Post-buckling deflection curves for different aspect ratios (a/b) of the laminated panel $(0/90/90/0)_s$.

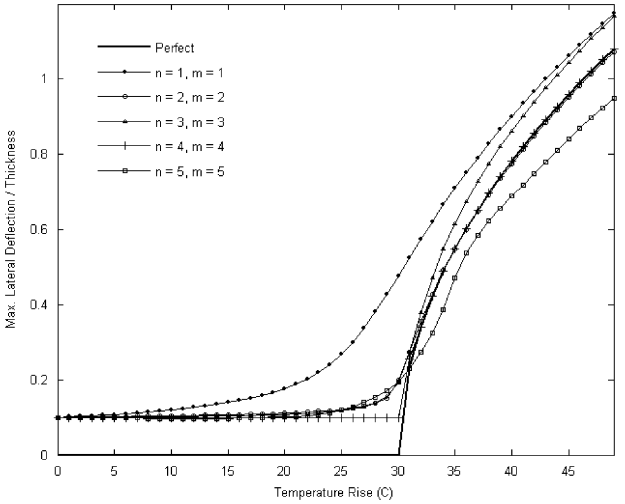

Fig. 5. Post-buckling deflection curves for a clamped composite panel with different half wave numbers in both x- and y-directions.

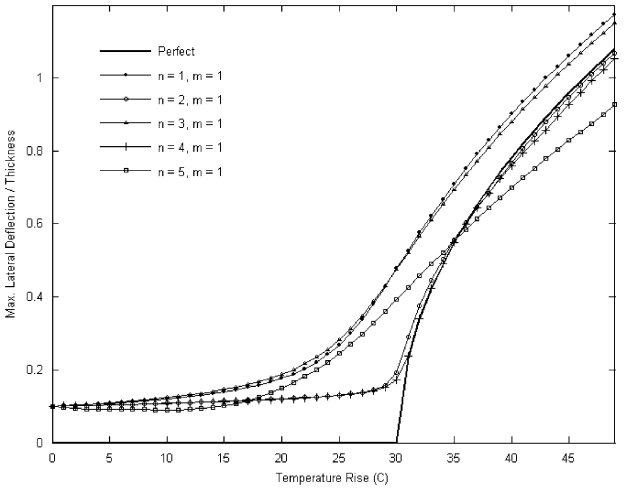

Fig. 6. Post-buckling deflection curves for a clamped composite panel with different half wave numbers in the x-direction.

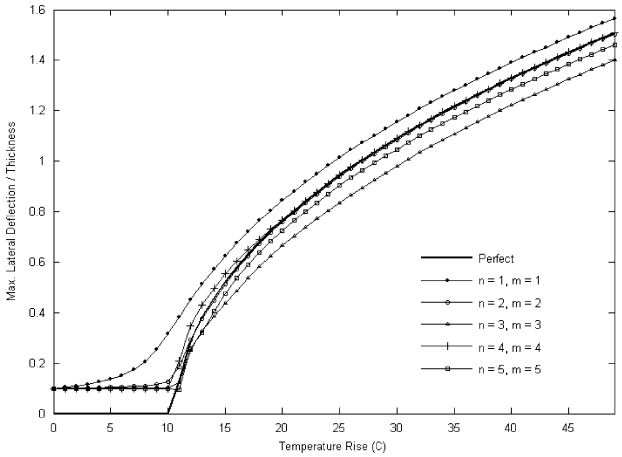

Fig. 7. Post-buckling deflection curves for a simply supported composite panel with different half wave numbers in both *x*- and *y*-directions.

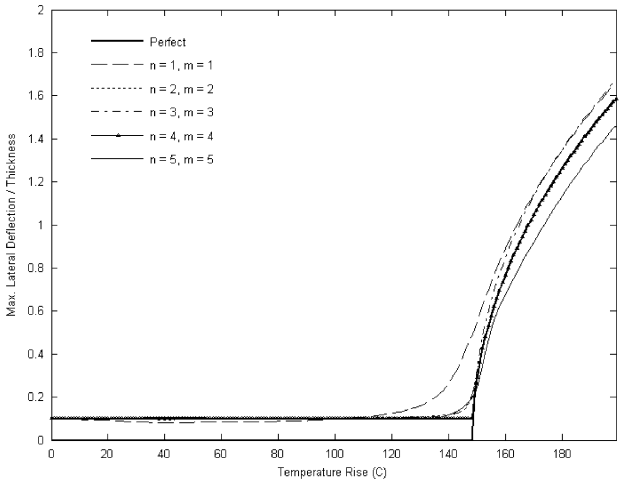

Fig. 8. Post-buckling deflection curves for a clamped SMAHC panel with different half wave numbers in both *x*- and *y*-directions.

response of an imperfect panel with a half wave number of 3 has lower post-buckling deflections than that of an imperfect panel with half wave number of 5.

The effect of SMA fiber embeddings on the thermal response of the clamped panel is presented in Fig. 8. Comparing the buckling equilibrium paths of the clamped SMAHC panels shown in Fig. 8 with those of Fig. 5, it is found that the SMA fiber embeddings offer a noticeable enhancement to the thermal stability of both perfect and imperfect panels through highly increasing the critical buckling temperature while completely hindering the thermal out-of-plane deflections of imperfect composite panels up to the vicinity of the buckling temperature. For an airflow of $\lambda = 50$, the aero-thermal behavior of both clamped and simply supported composite panels are shown in Figs. 9 and 10. It is seen in Fig. 9 that the presence of such airflow adds stiffness to both perfect and imperfect composite panels though slightly increasing the critical buckling temperature of the perfect panel along with decreasing the post-buckling deflections of all panels. Moreover, for symmetric imperfection shapes of multiple half waves, a qualitative difference in the response is noticed compared to those of Fig. 5. For the simply supported case presented in Fig. 10, the presence of airflow did not show a noticeable effect on the perfect panel response presented in Fig. 7, and this means that the chosen value of λ is much lower than the critical flutter value λ_{cr} [25]. In addition, the proposed imperfections with H equals 0.1 were found not to produce a pronounced deviation from the trend presented in Fig. 7.

4.3. Vibration behavior under aero-thermal loads

The natural frequency characteristics of imperfect composite panels with and without SMA fiber embeddings are investigated illustrating the effect of temperature rise, imperfection shape, boundary conditions and aerodynamic flow on

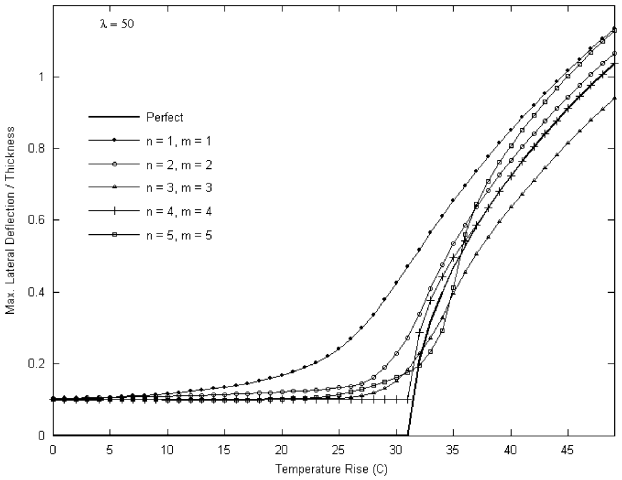

Fig. 9. Aero-thermal deflection curves for a clamped composite panel with different half wave numbers in both x- and y-directions and at $\lambda = 50$.

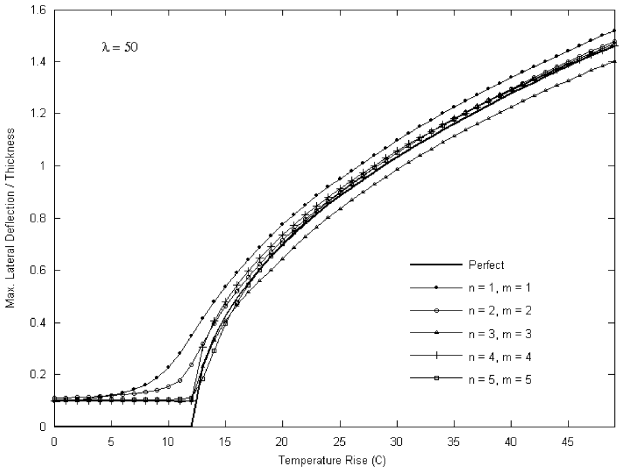

Fig. 10. Aero-thermal deflection curves for a simply supported composite panel with different half wave numbers in both x- and y-directions and at $\lambda = 50$.

the panel response. Figs. 11 and 12 present the fundamental frequency variation versus temperature rise for both clamped and simply supported imperfect composite panels. It is seen in Fig. 12 that the fundamental frequency decreases between room temperature (T_{ref}) and the critical buckling temperature (T_{cr}) due to the thermal expansion effect. At T_{cr}, the fundamental frequency of the perfect panel has a null value as the panel stiffness drops to zero at the critical buckling temperature. The fundamental frequency is seen to increase after passing T_{cr} because the nonlinear stiffness terms start to build up as a result of the increased post-buckling deflection. In addition, all imperfect panels almost have the same response before the occurrence of thermal buckling. After buckling, the panels with symmetric imperfection shapes are found to highly deviate from perfect panel performance. Moreover, it is observed that the presence of a small geometric imperfection may be favorable from the structural dynamics point of view through preventing the panel from having very low or null stiffness at the vicinity of the critical buckling temperature. Comparing the response of an imperfect simply supported composite panel shown in Fig. 12 to those of the clamped one, it is seen that the presence of a small sinusoidal imperfection does not result in a noticeable deviation from the behavior of the perfect panel except at the vicinity of the critical buckling temperature.

By including the effect of SMA fiber embeddings, the fundamental frequency behavior at elevated temperatures for both clamped and simply supported SMAHC panels are presented in Figs. 13 and 14. Fig. 13 reveals that the SMA constrained shape recovery stress overwhelms the thermal expansion effect at low temperatures making the panel stiffer, while showing different rates of fundamental frequency increase, because the recovery stress curve of the 3 percent pre-strain value has different increasing rates at this temperature range (see Fig. 3). The anti-symmetric imperfections still show deviated behavior in the vicinity and after the critical buckling temperature. If the edges are all simply supported, it is

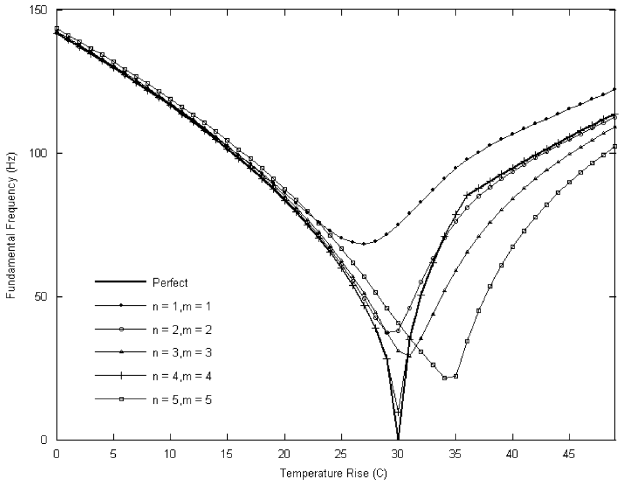

Fig. 11. Fundamental frequencies of a clamped composite panel with different imperfection modes versus temperature.

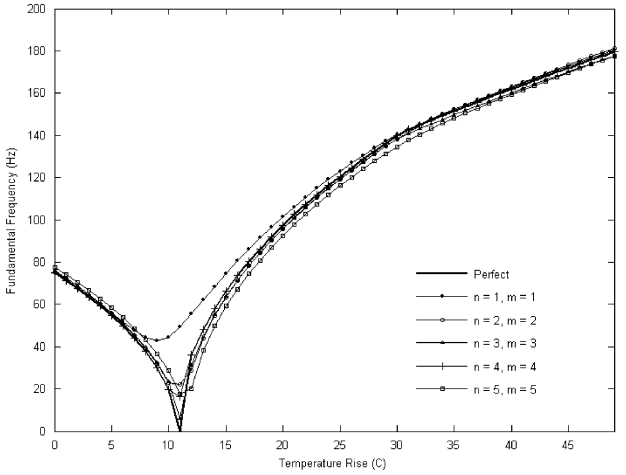

Fig. 12. Fundamental frequencies of a simply supported composite panel with different imperfection modes versus temperature.

observed in Fig. 14 that the geometric imperfections have no significant effect on the fundamental frequencies of the SMAHC panel except at the vicinity of the critical buckling, where the single half wave imperfection shows non-zero fundamental frequency.

A study for effect of having airflow along with elevated temperatures on the fundamental frequencies of imperfect simply supported and clamped composite panels are presented in Figs. 15–17. The fundamental frequency variation of an imperfect clamped composite panel exposed to airflow of $\lambda = 50$ and at elevated temperatures is presented in Fig. 15. Comparing the results to those of Fig. 11, it is found that the presence of airflow forced the anti-symmetric imperfection, which has 2 half waves in both directions, to highly deviate from the perfect panel response. In addition, imperfect panels having 3 and 5 half waves are seen to qualitatively differ in behavior compared to those of Fig. 11. Moreover, the presence of airflow is found to have no effect on the imperfect panel with 4 half waves since it is seen to have the same response of the perfect panel. For the simply supported composite panel presented in Fig. 16, the presence of airflow is found to have no noticeable effect on the fundamental frequencies of all imperfect panels except the one which has 2 half waves imperfection. Since it shows different response compared to the $\lambda = 0$ case presented in Fig. 12. Fig. 17 illustrates the fundamental frequency variation of the clamped composite panel versus the non-dimensional dynamic pressure λ and at different temperature rises. It is seen that increasing the value of λ have a stiffening effect through increasing the fundamental frequency of the panel. It is also found that, at temperature rises 0 and 20 °C, the presence of a small geometric imperfection with different shapes has no impact on the fundamental frequency variation. Meanwhile, in the vicinity of the buckling temperature, at a temperature rise 27 °C, the fundamental frequency is seen to be more sensitive to the imperfection shape especially at the lower values of λ.

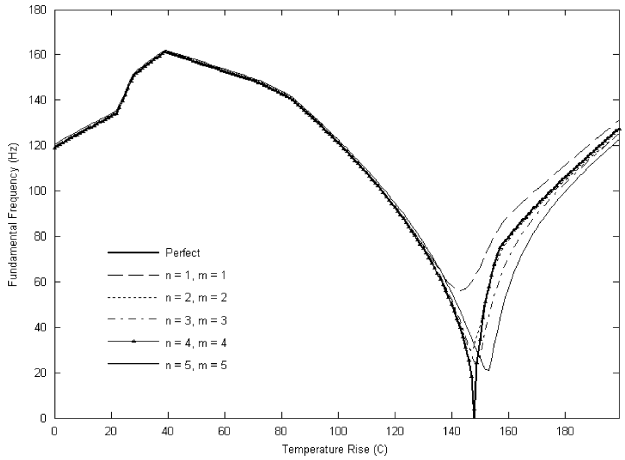

Fig. 13. Fundamental frequencies of a clamped SMAHC panel with different imperfection modes versus temperature.

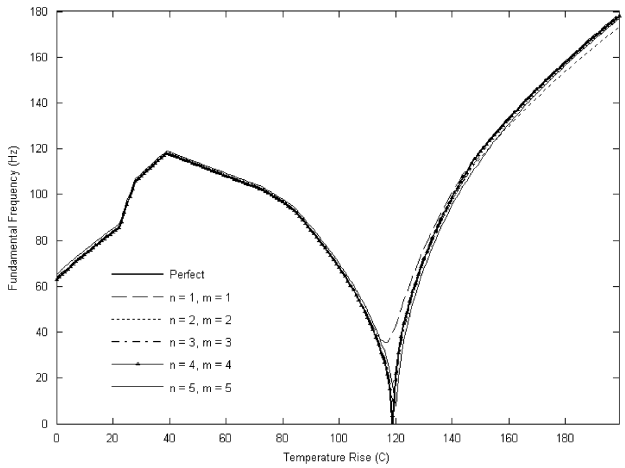

Fig. 14. Fundamental frequencies of a simply supported SMAHC panel with different imperfection modes versus temperature.

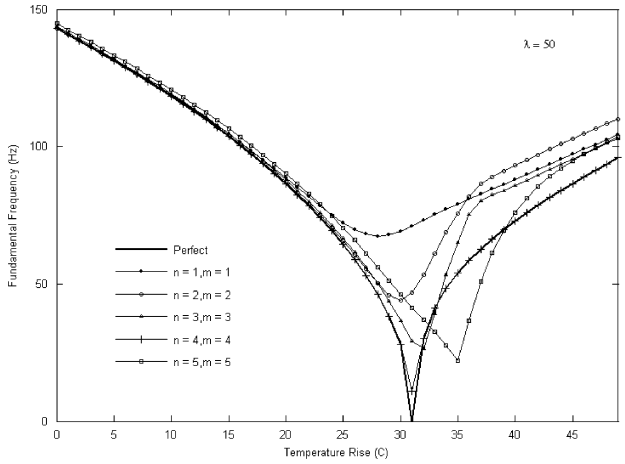

Fig. 15. Fundamental frequencies of a clamped composite panel with different imperfection modes versus temperature at $\lambda = 50$.

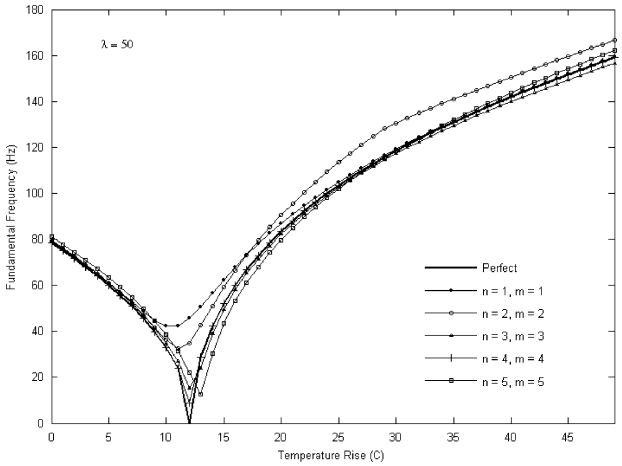

Fig. 16. Fundamental frequencies of a simply supported composite panel with different imperfection modes versus temperature at $\lambda = 50$.

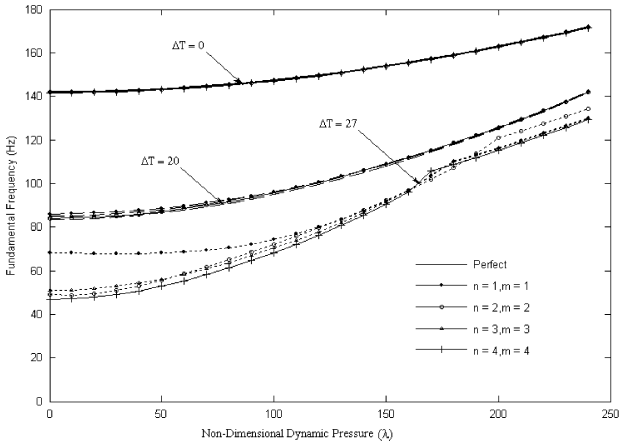

Fig. 17. Fundamental frequencies of a clamped composite panel versus the aerodynamic pressure λ at various temperature rises.

5. Conclusions

A nonlinear finite element model was provided to predict the static aero-thermal deflection and the vibration behavior of geometrically imperfect shape memory alloy hybrid composite panels under the combined effect of thermal and aerodynamic loads. The temperature-dependence of material properties for the composite matrix and SMA fibers was considered in the formulation. Newton–Raphson iteration method was employed to obtain the nonlinear deflections, while an Eigen value problem is solved at each temperature rise and non-dimensional dynamic pressure to predict the natural frequency for the corresponding deflected aero-thermal equilibrium position.

Results showed that shape memory alloy fiber embeddings can be very useful in controlling the panel fundamental frequency at elevated temperatures along with enhancing the thermal stability through increasing the buckling temperature and decreasing or suppressing the thermal post-buckling deflections. Shape memory alloy hybrid composite panels were found to have very low sensitivity to initial geometric imperfections compared to composite panels. It was observed that increasing the panel aspect ratio results in a more pronounced effect of the initial geometric imperfection. Composite panels with simply supported edges were found to be less sensitive to imperfections with multiple half waves compared to the clamped panels. Finally, in spite of having a deteriorating effect on aerodynamic performance, the presence of a small geometric imperfection may be favorable from the structural dynamics point view through preventing the panel from having very low or null fundamental frequencies at the vicinity of the critical buckling temperatures.

Acknowledgments

This work was supported by the BK21 Program, Hanyang University, Seoul, South Korea. The authors wish to express their gratitude for this financial support.

References

[1] T.R. Tauchart, Thermally induced flexure, buckling, and vibration of plates, *Applied Mechanics Review* 44 (1991) 347–360.
[2] E.A. Thornton, Thermal buckling of plates and shells, *Applied Mechanics Review* 46 (1993) 485–506.
[3] C.C. Gray, C. Mei, Finite element analysis of thermal postbuckling and vibrations of thermally buckled composite plates, *Proceedings of the 32nd AIAA/ASME/ASCE/AHS/ASC Structures, Structural Dynamics, and Materials Conference*, Part 4, AIAA, Washington, DC, 1991, pp. 2996–3007.
[4] R. Jones, J. Mazumdar, Vibration and buckling of plates at elevated temperatures, *Journal of Solid and Structures* 16 (1980) 61–70.
[5] Y. Shi, R.Y. Lee, C. Mei, Coexisting thermal post-buckling of composite plates with initial imperfections using finite element modal method, *Journal of Thermal Stresses* 22 (1999) 595–614.
[6] I.K. Oh, J.H. Han, I. Lee, Postbuckling and vibration characteristics of piezolaminated composite plate subject to thermo-piezoelectric loads, *Journal of Sound and Vibration* 233 (2000) 19–40.
[7] H.H. Ibrahim, M. Tawfik, M. Al-Ajmi, Aero-thermo-mechanical characteristics of functionally graded material panels with temperature-dependent material properties, *Proceedings of the Eighth International Congress of Fluid Dynamics and Propulsion* (*ICFDP8*), Sharm El-Shiekh, Egypt, American Society of Mechanical Engineers Paper ICFDP-EG-116, December 2006.
[8] H.H. Ibrahim, M. Tawfik, M. Al-Ajmi, Non-linear panel flutter for temperature-dependent functionally graded material panels, *Computational Mechanics* 41 (2008) 325–334.
[9] H.H. Ibrahim, M. Tawfik, M. Al-Ajmi, Thermal buckling and nonlinear flutter behavior of functionally graded material panels, *Journal of Aircraft* 44 (2007) 1610–1618.
[10] V. Birman, Review of mechanics of shape memory alloy structures, *Applied Mechanics Review* 50 (1997) 629–645.
[11] H.J. Lee, J.J. Lee, A numerical analysis of the buckling and postbuckling behavior of laminated composite shells with embedded shape memory alloy wire actuators, *Smart Materials and Structures* 9 (2000) 780–787.
[12] M. Tawfik, J.J. Ro, C. Mei, Thermal post-buckling and aeroelastic behavior of shape memory alloy reinforced plates, *Smart Materials and Structures* 11 (2002) 297–307.
[13] J.H. Roh, I.K. Oh, S.M. Yang, J.H. Han, I. Lee, Thermal postbuckling analysis of shape memory alloy hybrid composite shell panels, *Smart Materials and Structures* 13 (2004) 1337–1344.
[14] J.S. Park, J.H. Kim, S.H. Moon, Vibration of thermally post-buckled composite plates embedded with shape memory alloy fibers, *Composite Structures* 63 (2004) 179–188.
[15] H.H. Ibrahim, M. Tawfik, H.M. Negm, Thermal post-buckling and flutter behavior of shape memory alloy hybrid composite plates, *Proceedings of the Eighth International Congress of Fluid Dynamics and Propulsion* (*ICFDP8*), Sharm El-Shiekh, Egypt, American Society of Mechanical Engineers Paper ICFDP-EG-153, December 2006.
[16] H.H. Ibrahim, M. Tawfik, H.M. Negm, Thermoacoustic random response of shape memory alloy hybrid composite plates, *Journal of Aircraft* 45 (2008) 962–970.
[17] Y. Shi, R.Y. Lee, C. Mei, Thermal post buckling of composite plates using the finite element modal coordinate method, *Journal of Thermal Stresses* 22 (1999) 595–614.
[18] H.-S. Shen, Thermal postbuckling behavior of shear deformable FGM plates with temperature-dependent properties, *Computer Methods in Applied Mechanics and Engineering* 190 (2001) 5377–5390.
[19] J. Girish, L.S. Ramachandra, Thermal postbuckling vibrations of symmetrically laminated composite plates with initial geometric imperfections, *Journal of Sound and Vibration* 282 (2005) 1137–1153.
[20] B.A. Shariat, M.R. Eslami, Thermal buckling of imperfect functionally graded plates, *Solids and Structures* 43 (2006) 4082–4096.
[21] B. Mirzavand, M.R. Eslami, Thermal buckling of imperfect functionally graded cylindrical shells based on the Wan-Donnell model, *Journal of Thermal Stresses* 29 (2006) 37–55.
[22] C.C. Chen, C.Y. Hsu, Imperfection sensitivity in the nonlinear vibration oscillations of initially stressed plates, *Applied Mathematics and Computation* 190 (2007) 465–475.
[23] H.-S. Shen, Thermal postbuckling behavior of shear deformable FGM plates with temperature-dependent properties, *International Journal of Mechanical Sciences* 49 (2007) 466–478.
[24] F.K. Bogner, R.L. Fox, L.A. Schmit, The generation of inter-element compatible stiffness and mass matrices by the use of interpolation formulas, AFFDL-TR-66-80, Wright-Patterson AFB, OH, 1966, pp. 396–443.
[25] M.S. Azzouz, Nonlinear Flutter of Curved Panels Under Yawed Supersonic Flow Using Finite Elements, PhD Thesis, Old Dominion University, Mechanical Engineering Department, Norfolk, Virginia, 2005.
[26] ENV 1993-1-6, Eurocode 3: Design of steel structures, Part 1.6: General rules—supplementary rules for the strength and stability of shell structures, CEN, Brussels, 1999.
[27] D.Y. Xue, Finite Element Frequency Domain Solution of Nonlinear Panel Flutter with Temperature Effects and Fatigue Life Analysis, PhD Thesis, Old Dominion University, Mechanical Engineering Department, Norfolk, Virginia, 1991.
[28] W.B. Cross, A.H. Kariotis, F.G. Stimeler, Nitinol characterization study, NASA CR-14B, 1969.